Available online at www.sciencedirect.com
ScienceDirect
Journal of Fluorine Chemistry 128 (2007) 353–368
JOURNAL OF FLUORINE CHEMISTRY
www.elsevier.com/locate/fluor

Review

Non-aqueous sol–gel synthesis of nano-structured metal fluorides

Stephan Rüdiger, Udo Groß, Erhard Kemnitz *

Humboldt-University Berlin, Institute of Chemistry, Brook-Taylor-Str. 2, D-12489 Berlin, Germany

Received 29 August 2006; received in revised form 9 November 2006; accepted 13 November 2006
Available online 18 November 2006

Dedicated to Karl Christe's 70th birthday.

Abstract

This review summarises the progress, achieved in the last 5 years, in the field of synthesis of nano-structured metal fluorides. The main focus is laid on the non-aqueous sol–gel-synthesis, which is opening a wide window toward nanoscopic metal fluorides with properties remarkably different from that of crystalline metal fluorides. Based on examples of binary as well as complex metal fluorides prepared via this new sol–gel-route it will be shown how the physical properties of nanoscopic compounds deviate from their macroscopic counterparts.

Keywords: Sol–gel-synthesis; Nano-structured metal fluorides; Cataylsis; Lewis acidity; Optical properties

Contents

* Corresponding author. Tel.: +49 30 2093 7555; fax: +49 30 2093 7277.
E-mail addresses: erhard.kemnitz@chemie.hu-berlin.de, erhard.kemnitz@rz.hu-berlin.de (E. Kemnitz).

0022-1139/$ – see front matter © 2006 Elsevier B.V. All rights reserved.
doi:10.1016/j.jfluchem.2006.11.006

1. Introduction

Miniaturisation is a prevailing trend in science and technology. Microelectronics has approached a critical structure dimension of 0.18 μm. With the nanometer scale we have entered into dimensions not too much different from the atomic or molecular dimension (1 Å = 0.1 nm). Just to imagine these dimensions: the diameter of a louse is about 1 mm, that of a bacteria by the factor 1000 smaller (∼1 μm), but an influenca virus is about 10,000 times smaller (∼0.1 μm = 100 nm). Hence, the nanometer scale has become the borderline of different disciplines like chemistry, physics, and biology.

Nanotechnology is about to change science and technology, and hence our life fundamentally comparable with the impact of microelectronics on our life over the past 30 years. Nanoscience and technology have already gained technology ready applications as for instance nanoscopic metal oxides, nanosized metals, or nanoscopic inorganic–organic hybrid systems, respectively [1].

Materials properties are discussed for units consisting of some 10^{23} building blocks (atoms, molecules, ions, etc.). However, properties of single atoms deviate from macroscopic materials. Thus, e.g., the magnetization and demagnetization, respectively, of Fe is impossible with single Fe-atoms because this demands an ensemble of a certain number of Fe atoms. The dimensions of nano-particles, some few up to some 100 nm, are between those of single atoms and macroscopic materials. Hence, materials properties very often show distinct changes when particle size falls below a critical value. There are two major reasons for this size-dependent behaviour of materials: (i) the surface effect and (ii) the volume effect or size quantization, which will be briefly reflected on the example of a metal:

(I) The surface effect occurs generally with every surface atom of any material. In case of a metal, the common coordination number of a bulky atom is 12. However, atoms at the surface are coordinatively under-saturated, and hence, exhibit a lower coordination number than their bulk-counterparts. As a result of these non-saturated bonds, surface atoms exist in a kind of excited energy level. Since for macroscopic dimensions of a materials particle the percentage of surface atoms is very low, we usually do not realise it, although this effect exists always. Reduction of the particle size to nanometer scale results in a different situation. The percentage of surface atoms can exceed that of bulky atoms, i.e. the materials properties of such small particles are no longer determined by coordinatively saturated bulk-atoms but by under-saturated surface atoms as shown convincingly in Table 1 in going from 500 to 1 nm particle size.

As a result of this surface effect, such nano-particles are excellent adsorbers, heat exchangers, and sensors, respectively.

(II) The volume effect reflects the energy state of binding electrons in nanoscopic solids, e.g., the energy state of binding electrons in simple bi-atomic molecules can easily be described based on the molecular orbital theory, which defines binding and anti-binding MOs in the molecule representing discrete energy levels of electrons. To describe the energetic situation in a macroscopic three-dimensional solid, the band theory is the most used theory, which describes the existence of electrons in more or less wide energy bands. In other words, there is no discrete energy state for each single electron. Starting from such a macroscopic solid characterised by a certain band structure and reducing the size of this solid step by step, certainly a critical size will be reached at which the band structure no longer exists. From this point (usually, when the particles become smaller than the Debye-wave length, e.g., for Si: 41.5 nm), we will observe an increase of the band gap (quantum dots). As a consequence, the electronic properties of a material, although it is chemically still the same, may deviate fundamentally from that of the macroscopic unit.

Table 1
Estimated relative part of atoms at the surface depending on the size of the particle

Particle size (nm)	Total number of atoms	Part of surface atoms (%)
500	3.45×10^9	1
50	3,400,000	3.5
5	3,430	32
1	34	94

From this brief introduction it is obvious that the smaller the particles the more reactive they are. Consequently, it is not an easy task to synthesize nano-sized particles because, from the thermodynamic point of view, the formation of bigger crystals is definitely favoured, since this leads to the formation of more stable phases.

2. Synthesis strategies for nano-metal fluorides

Several syntheses of nano-metal fluorides have been developed and are used, which include physical as well as chemical methods.

Physical methods are condensation of nano-materials from a suitable vapour phase, e.g., PbF_2 [2], mechanical milling, e.g., FeF_3 and GaF_3 [3], laser dispersion, e.g., NaF [4], and molecular-beam epitaxy for coatings, e.g. [5,6].

Chemical methods have been explosively developed over the last 5 years, such as pyrolysis of suitable fluorinated precursor materials (cf. [7] and references therein) and sol–gel synthesis. Sol–gel synthesis is unambiguously the most powerful synthesis route towards nano-sized materials [8].

For the pyrolysis route, mostly metal trifluoroacetates (TFA) are used, but also other F-containing thermally unstable compounds might be used. Hence, the principal of the pyrolysis strategy will briefly be reflected while discussing the TFA-sol–gel synthesis procedure.

2.1. The general principle of a sol–gel synthesis

The general reaction path of this method consists in the condensation reaction of terminal hydroxyl-groups (Eq. (1)):

$$M{-}OH + HO{-}M \rightarrow M{-}O{-}M + H_2O \quad (1)$$

In order to control the speed of condensation and to prevent the system from precipitation, usually one starts from controlled hydrolysable precursors, the most prominent of these are metal alkoxides. Starting from alkoxides, the reaction can be stopped on the stage of sol-formation by controlling the reaction conditions (pH, type of alkoxide, temperature, concentration, etc.):

$$M{-}OR + H_2O \rightarrow M{-}OH + ROH \quad (2)$$

Thus, it is possible to control subsequent condensation reactions according to Eqs. (1) or (3), preventing the primary particles from further condensation (in a ideal case, a sol is formed):

$$M{-}OR + HO{-}M \rightarrow M{-}O{-}M + ROH \quad (3)$$

From the primary sol one may get the wet gel, consisting usually of up to 85% of the solvent and just maximum 15% of the solid. Further treatment results in dry gels of the respective metal oxide. However, this sol–gel synthesis, per definition, results always in the formation of metal oxides, which are of interest and used for many applications.

On the other hand, for several applications metal fluorides are significantly better candidates than their oxidic counterparts, as in optics (better transmittance, diffraction indices), laser applications, hydrophobic coating, surface sealing, solid Lewis acids, etc.

Hence, there have been many activities to develop synthesis strategies leading to metal fluorides via sol gel route.

These methods can be divided principally into two groups.

2.2. Chemical methods to nano-sized metal fluorides

2.2.1. Post-fluorination of a metal oxide prepared via a sol–gel-route

The general procedure consists in the preparation of a metal oxide according the classical sol–gel procedure followed by a post-fluorination as simplified in Scheme 1.

This way, several pure and doped metal fluorides (oxofluorides) have been synthesized and investigated, especially regarding their optical properties [9–18]. The disadvantage of this procedure is that HF and other toxic gases are released during calcination, that it results in a dramatic decrease of the surface area of the metal fluoride (accompanied often with the loss of nano-dimension!), and incomplete conversion of the metal oxide, i.e. formation of multi-phase systems [19].

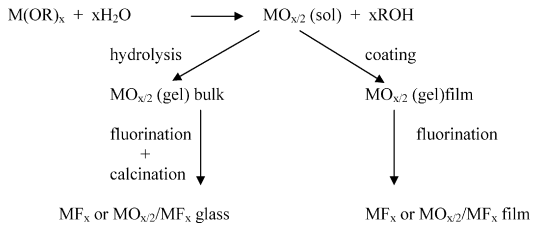

Scheme 1. Metal fluoride preparation via post-fluorination of sol–gel prepared metal oxides.

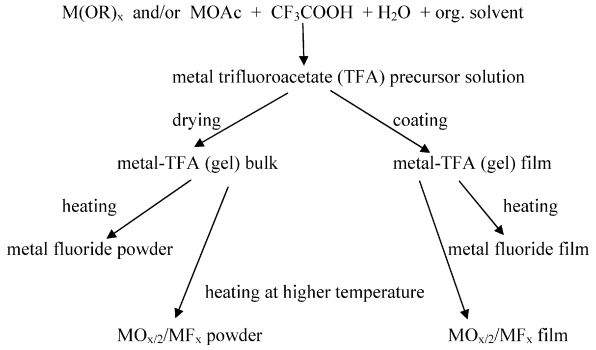

Scheme 2. Metal fluoride preparation via metal fluoroacetate sol–gel formation and following thermal decomposition.

2.2.2. Sol–gel formation of metal trifluoroacetates and their thermal decomposition

This method consists in reacting an alcoholic metal alkoxide solution with aqueous trifluoroacetic acid resulting in a metal trifluoroacetate sol to be used for, e.g., coating, followed by drying and necessarily by thermal decomposition, which, in some cases, results in the formation of metal fluorides, in some other cases in the formation of oxofluorides but in many other cases in the formation of mixtures of oxides and fluorides (cf. Scheme 2).

This way, several nano-metal fluorides have been prepared, which, again, were mainly investigated regarding their potential application for optical devices.

The disadvantages of this method are the restriction on such metals for which fluoroacetates exist, the unwanted formation of multi-phase systems (in several cases, containing often organic residues) and the possible increase of size beyond nanoparticle size due to the high temperatures necessary for thermal decomposition of the TFA. This method has been extensively investigated and developed by Fujihara and has been reviewed recently, hence we refer to this review article [20] and references therein for further information.

3. Non-aqueous sol–gel synthesis

3.1. Synthesis route

The sol–gel fluorination synthesis of metal fluorides and related materials is subject of several papers and patents [21–32]. Typically, synthesis, as shown schematically in Scheme 3, starts from metal alkoxides [21], though other metal compounds have also been reported [22–24] and claimed [30].

The alkoxide is dissolved or dispersed in alcohol or another non-aqueous solvent and the calculated amount of HF dissolved in alcohol or diethyl ether is added under vigorous stirring. Depending on type of metal and on concentrations used a metal fluoride in alcohol sol/gel is formed. The latter can either

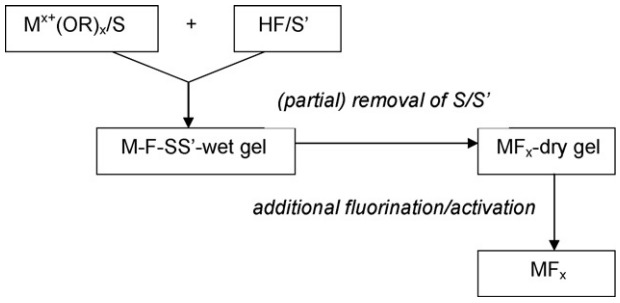

Scheme 3. Metal fluoride synthesis via non-aqueous sol–gel fluorination.

directly be used for, e.g., coatings [31], or dried to yield solid, powdery metal fluorides. In case that highly Lewis acidic metal ions are involved, such as Al^{3+}, the dried material has to undergo an additional treatment with a gaseous fluorinating agent at elevated temperatures (see Scheme 3) to get a pure AlF_3 with high surface area (HS-AlF_3) and exceptional high Lewis acidity [21,25,29]. Because of the outstanding Lewis acidity of HS-AlF_3, the influence of a great many of parameters on the HS-AlF_3 synthesis has been studied in detail aiming optimisation of the process. These include nature of alkoxidic group and of solvent, concentration, molar ratio of metal ion to HF, gel ageing, method of gel drying, nature and concentration of gaseous fluorinating agent, temperature regime [29]. In accordance with [29] and Scheme 3 these parameters will be discussed in condensed form in the following order: wet gel formation, transforming wet gel into dry gel, post-fluorinating activation.

The concentration of metal alkoxide has no distinct effect on the properties of the final metal fluoride, only the gel formed becomes more stiffer with increasing concentration. Likewise, with the Al^{3+}:HF ratio varied from 1:2 up to 1:4 amorphous HS-AlF_3 could be obtained, obviously under-stoichiometric amounts of HF could be balanced by the second fluorination/activation step, which is necessary in case of HS-AlF_3. An even higher excess of HF than Al:HF equal to 1:4 resulted, however, in formation of crystalline AlF_3 having a rather low surface area. Reacting $Al(O^iPr)_3$ in ^{i}PrOH with stoichiometric amounts of HF, i.e. under standard conditions, there was no substantial difference in outcome starting from room temperature or from −70 °C. In contrast to the parameters already discussed, nature of alkoxidic group and of solvent have a somewhat more pronounced influence on the reaction. In going from Al-methoxide/MeOH over Al-isopropoxide/^{i}PrOH to Al-*tert*-butoxide/*n*-BuOH, the specific surface area of the HS-AlF_3 prepared increased from about 200 m^2/g to about 320 m^2/g, although the Lewis acidity of all these AlF_3 samples was almost alike, i.e. extremely high. With methanol as reaction medium the primary product tends to be a sol rather than a gel as in case of isopropanol, even at distinctly higher alkoxide concentrations. However, upon concentrating, that is removal of alcohol, the sol becomes a wet and finally a dry gel independent on the alcohol used. Similar observations have been reported for the magnesium fluoride system, too [26]. Instead of alcohol as reaction medium the use of, e.g., toluene [25] or tetrahydrofurane [28] has also been described.

From the sol or wet gel the solvent, i.e. the alcohol has been removed in order to obtain a dry gel by evacuation at elevated temperatures up to 70 °C as well as by freeze-drying, the HS-AlF_3 prepared from the dry gels were almost identical. Dry Al–F-gel prepared by vacuum drying at temperatures up to 100 °C had a surface area up to 600 m^2/g. In contrast to these work-up procedures, ageing the wet gel at room temperature over altogether 120 days had a distinct influence on its properties, probably because of processes resulting in somewhat more regular structure of the gel, whereby the gel volume is shrinking and some part of the alcohol becomes a separate layer. Both, surface area and Lewis acid dependent catalytic activity of the HS-AlF_3 prepared from the aged gel became reduced with ageing time [29].

A dry gel of aluminium fluoride (the ‘‘precursor’’ in some of the papers cited) prepared as described above contains always substantial amounts of alcohol and/or alkoxidic groups mounting up to an analytical carbon content of 30%. Thermoanalysis showed the stepwise release of firstly more weakly bound alcohol followed by more tightly bound alcohol and/or alkoxide groups (Fig. 1).

In going from AlF_3 to MgF_2 [26] and to NaF [28] the carbon content of the dry gel goes down to less than 1%. This shows that the Lewis acidity of the metal cation in its fluoridic environment is responsible for the degree of solvent binding. At the same time the organic constituents are covering and blocking preferably the strongest Lewis acid sites. To remove the organic constituents from aluminium fluoride dry gel aiming at preparation of the extremely highly Lewis acidic HS-AlF_3, simply heating of the dry gel in an inert gas is not successful but heating in a flow of a gaseous fluorinating agent has proven to be useful [21,25,29]. This process, named activation because the catalytically inactive dry Al–F-gel becomes a very active catalyst, has been investigated in detail aiming its optimisation [29]. As fluorinating agents fluorocarbon compounds as well as HF have been tested under varied reaction conditions, such as concentration, temperature, and reaction time. As fluorinating agents CCl_2F_2, $CHClF_2$ and HF have been successfully employed, whereas CH_2F_2 and CH_2FCF_3 caused extensive coke formation on the aluminium fluoride, obviously because of lower stability of these

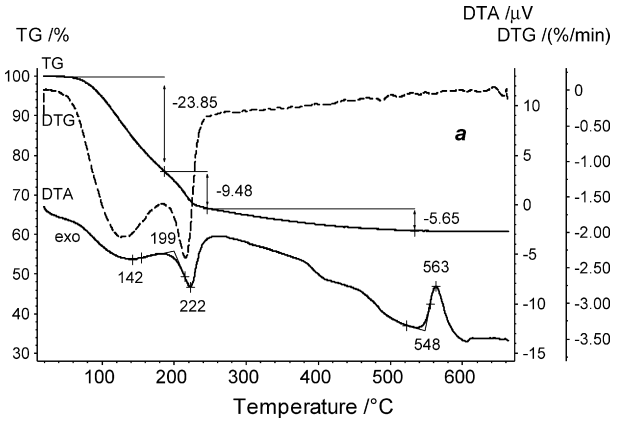

Fig. 1. Thermoanalysis of a dry Al–F-gel (reproduced from [25] by permission of The Royal Society of Chemistry).

Table 2
Influence of temperature on activation of dry Al–F-gel with $CHClF_2$[a]

Sample	Fluorination temperature (°C)	BET-surface area (m^2/g)	1,2-DBP isomerisation activity (%)[b]
1	25–250	250–309	≈90
2	25–300	188	54
3	25–350	155	28

[a] Based on data taken from [29].
[b] Isomerisation of 1,2-dibromohexafluoropropane to 2,2-dibromohexafluoropropane (see below).

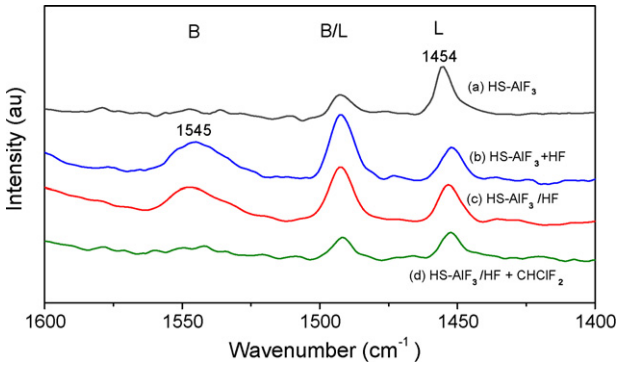

Fig. 2. PAS of pyridine adsorbed on (a) HS-AlF_3, (b) HS-AlF_3 exposed to HF, (c) HS-AlF_3/HF, and (d) HS-AlF_3/HF heated in $CHClF_2/N_2$; peaks at (B) are indicative for Brønstedt acidity, and peaks at (L) for Lewis acidity (reproduced from [29] Fig. 10 by permission of Springer Publishers).

compounds due to their higher hydrogen content. The first reported synthesis of the highly Lewis acidic, amorphous HS-AlF_3 [21] was performed with CCl_2F_2 and $CHClF_2$, respectively. The reactions were carried out in a tube-type flow reactor. Temperatures up to 300 °C (with CCl_2F_2) or 250 °C ($CHClF_2$; Table 2) were necessary to obtain highly Lewis acidic amorphous HS-AlF_3 having a specific surface area of about 200–300 m^2/g. The reaction with CCl_2F_2 was studied in detail by online GC/MS, whereby both products resulting from the fluorination reaction, i.e. $COCl_2$, as well as from dismutation reaction of CCl_2F_2 indicating successful activation, i.e. high Lewis acidity of the aluminium fluoride, were observed [25]. Applying lower temperatures a higher surface area was observed together with incomplete removal of the organic material and, consequently, no or low Lewis acidity, the latter was estimated on the basis of the catalytic performance in test reactions depending on Lewis acidic catalysts (Table 2). Higher temperatures (up to 400 °C) resulted in smaller surface area and lower catalytic activity of the AlF_3, which, however, remained amorphous.

Gaseous HF as the most simple and obvious fluorinating agent was also tested as post-fluorinating/activating agent [25,29]. Because of its higher fluorinating activity HF can be used at rather low temperatures whereby the very high surface area of the dry gel can be preserved to a large extent. Low HF concentration and a temperature of about 120 °C are optimum for preparing an aluminium fluoride, named HS-AlF_3/HF, with high surface area and low carbon content. However, in contrast to HS-AlF_3, HS-AlF_3/HF is not a highly Lewis acidic catalyst. It was shown [25,29] that this is caused by HF strongly attached to and therefore blocking the strongest Lewis acid sites and creating Brønstedt acidity. Fig. 2 shows the effect of HF adsorbed on HS-AlF_3 as well as in HS-AlF_3/HF together with the effect of a post-treatment of HS-AlF_3/HF with $CHClF_2$ as a way to gain high Lewis acidity. The re-activation of HS-AlF_3/HF to HS-AlF_3 can also be done by heating in an N_2 flow [29].

3.2. Synthesis mechanism

Although investigations to understand the mechanism of the sol and gel formation in detail are still in progress, to some extent information has already gained regarding the mechanism of direct sol–gel fluorination.

The overall reaction of an aluminium alkoxide with HF dissolved in iso-propanol, HO^iPr, is considered simply as a proton initiated nucleophilic substitution reaction replacing OR by F as summarily shown for the tetrameric Al isopropylate in the following equation:

$$Al_4(O^iPr)_{12} + 12HF \rightarrow 4AlF_3 + 12(CH_3)_2CHOH \quad (4)$$

The schematic structure model of the process with ongoing degree of fluorination from tetrameric aluminium iso-propoxide (a) to polymeric distorted aluminium fluoride (d) is shown in Scheme 4.

Evidence of the above assumption is emphasized also by a crystal structure determination of a compound with the first fluorine atom in a molecular entity (Scheme 4b) of the reaction chain [25].

Having in mind that the aluminium tris-isopropoxide exists as tetramer, $Al_4(O^iPr)_{12}$, with one octahedral and three tetrahedral Al sites (Scheme 4a), the detailed course of reaction is clearly of much higher complexity of transition states and

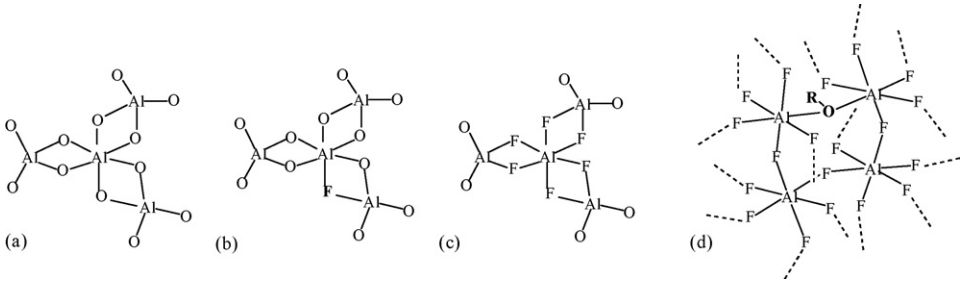

Scheme 4. Structure models. (a) $Al_4(O^iPr)_{12}$, (b) partially fluorinated, (c) $Al(OR, F)_6$ intermediate, and (d) Al alkoxide fluoride (reproduced from [25] by permission of The Royal Society of Chemistry).

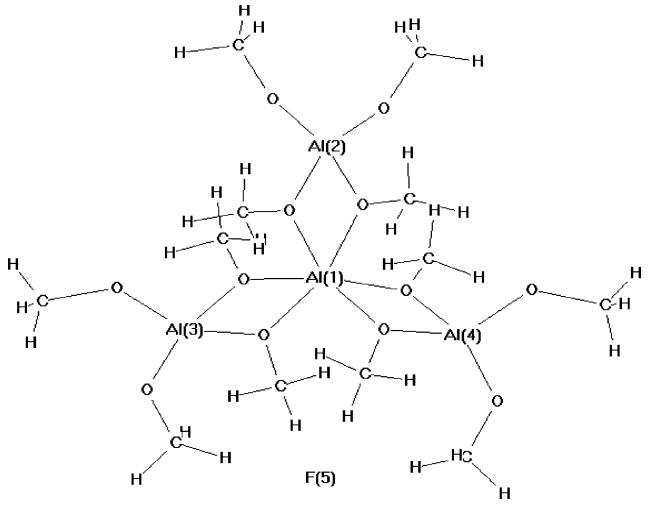

Fig. 3. F-complex.

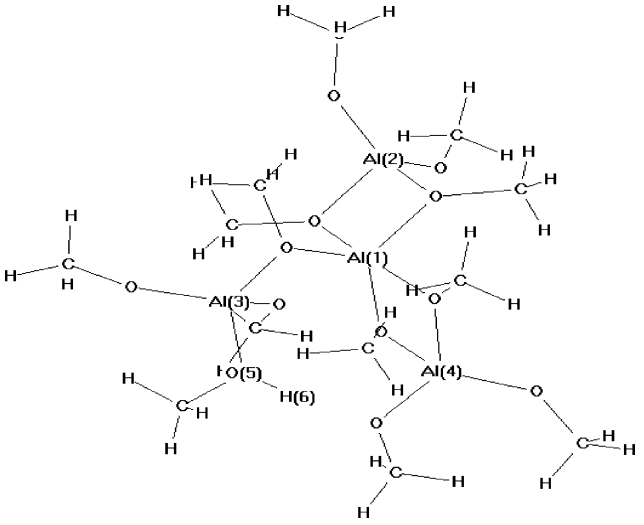

Fig. 4. H-complex.

intermediates than the reaction type of S_{N1} simply implies. Therefore, a study was executed to simulate the reaction mechanism of the aluminium alkoxide non-aqueous HF fluorination by DFT quantum chemical calculations [33]. The calculations were performed with the B3LYP functional and different basis sets to follow probable steps of introduction of fluorine. To test the model the structure of aluminium tris-isopropoxide tetramer was calculated. The obtained results are close to the experimental crystal structural data. Fig. 3 points out the calculated structure, for simplification the iso-propoxy groups are replaced by methoxy groups, and atom #5 of the image is a fluoride ion entering the system as first reactant.

Two principal routes of model reactions were considered for simulation: (i) starting the first reaction step with fluoride ion and (ii) starting with the protonation step, well knowing that the HF-solvent does not contain neither naked proton nor naked fluoride. As it is known, HF occurs as poly-hydrogen fluoride $(HF)_n$, which self-dissociates according to the equilibrium:

$$(HF)_n \leftrightarrows H_2F^+ + [F(HF)_{n-2}]^- \quad (5)$$

$$[HF]_n + HO^iPr \leftrightarrows [F\cdots H]_n \cdots\cdots O(H)^iPr \rightleftarrows O^+H_2{}^iPr + [F(HF)_{n-1}]^- \quad (6)$$

Additionally, the solvated proton of Eq. (5) in admixture with alcohol or ether as solvents is often proposed as ionic according to the Meerwein-type acidic oxonium ions (Eq. (6)). Results of Olah and co-workers [34] indicate the existence of hydrogen-bonded acid–base-complexes, while ionic states are discussed as border line cases only.

Following the route (i) of adding F^- ion to the system, the ion is fixed at the iso-propoxy group by hydrogen bonding (Fig. 3, F-complex). The mean distance d(C–H$\cdots$F$^-$) between F and C linked to the bridged oxygen atom is 296 pm. The complex is at a global minimum at the potential hyper surface and probably able to be isolated. Concurrently, the H^+ is protonating the bridging oxygen next to F with concomitant ring opening. The first fluorine atom enters the peripheral Al atom to become covalently bound. The alcohol molecule is set free, but remaining in the coordination sphere of the metal. Next step is the replacement of the alcohol by a second fluorine, making the central Al atom again six-fold coordinated. Pathway (ii) differs in that the primary step of attack is protonation of bridging oxygen forming the H-complex (Fig. 4). Consequently, the bridge is opened and the coordination number at central Al decreases to 5.

The fluoride ion will be predominantly bound covalently to the five-fold coordinated Al with ring closure, while the alcohol remains attached to the peripheral Al.

The DFT simulations leads to the conclusions in agreement with the experiment that [33]:

- protonation is the predominating step;
- only protonation of the bridging oxygen results in ring opening and further reaction;
- alcohol once freed remains in the vicinity of peripheral Al.

Thus, the preconditions for an open network structure and for gel formation are created. The partial occupation of binding sites by alkoxo groups and/or alcohol causes a mainly hydrogen-bonded meta-stable framework of gel structures that prevent the thermodynamically favoured crystallisation of AlF_3. Therefore, this material is highly distorted and X-ray amorphous. Due to the mesoporous morphology of the solid the surface area is extremely high.

Principally, the mechanistic considerations of the reaction path for AlF_3 are applicable also to other metal fluorides, e.g., MgF_2. Observed differences may be the result of different strength of solvate complexes, which depends on Lewis acidity of the metal fluorides.

Magnesium fluoride is considered as a non-acidic metal fluoride and obtained by the sol–gel reaction similarly, e.g., from the methoxide solvate $Mg(OCH_3)_2{\cdot}2CH_3OH$ [35], which structure is that of a tetrameric Mg–O–heterocubane spatial arrangement with oxygen in bridging and terminal positions. Thus, the above described calculation model can principally be applied to the related structure of the magnesium alkoxide and probably others, too.

3.3. Examples of binary metal fluorides

Till now the non-aqueous sol–gel fluorination route has been successfully employed for the synthesis of aluminium fluoride (HS-AlF_3), which is because of its exceptional properties most thoroughly investigated [21,25,29], magnesium fluoride (HS-MgF_2) [26], LiF, NaF, KF, CsF [28], CaF_2, BaF_2, ZnF_2 [36], PbF_2 and ZrF_4 [42].

HS-AlF₃: The synthesis of HS-AlF_3 follows the route described above, i.e. firstly $Al(OR)_3$ is subject to sol–gel fluorination and secondly the Al–F-gel obtained has after drying to be further fluorinated and thereby activated [21]. Investigations aiming at optimisation of HS-AlF_3 synthesis [29] suffered from the drawback that there is no straightforward measure for its quality. Specific surface area and carbon content are helpful for an evaluation of HS-AlF_3, but for obvious reasons the strength of Lewis acidity would be the real measure, however, it can not be directly determined. Therefore, as indirect measures catalytic reactions have been selected which depend specifically on the action of Lewis acidic catalysts [29]. As such reactions were dismutation of CCl_2F_2 (Eq. (7)) [21] or $CHClF_2$ (Eq. (8)) [25] and isomerisation of CCl_2FCClF_2 (Eq. (9)) [37] and of $CBrF_2CBrFCF_3$ (Eq. (10)) [21] used. The two dismutation reactions proceed in the presence of catalysts showing moderate Lewis acidity, but the two isomerisation reactions need very strong Lewis acidic catalysts. Thus, $CBrF_2CBrFCF_3$ isomerises only in the presence of aluminium chlorofluoride or, at elevated temperatures, antimony pentafluoride, but also with HS-AlF_3 already at room temperature, giving evidence for the exceptional high Lewis acidity of HS-AlF_3, which has to be regarded as solid superacid:

$$5CCl_2F_2 \rightarrow CClF_3 + 3CCl_3F + CCl_4 \quad (7)$$

$$3CHClF_2 \rightarrow CHCl_3 + 2CHF_3 \quad (8)$$

$$CCl_2FCClF_2 \rightarrow CCl_3CF_3 \quad (9)$$

$$CBrF_2CBrFCF_3 \rightarrow CF_3CBr_2CF_3 \quad (10)$$

Reaction (9), isomerisation of CCl_2FCClF_2, which is of technical interest, was studied in more detail [37]. It could be shown that $AlCl_3$, which is known to be useful in batch reactions with liquid CCl_2FCClF_2 only, is not able to catalyse the isomerisation unless it had become converted by the fluorinating action of CCl_2FCClF_2 in the much more active aluminium chlorofluoride (ACF). In contrast, HS-AlF_3 was immediately active both in liquid as in gas phase reactions. Computational investigations showed that in the regularly ordered $AlCl_3$ all Al atoms next to the surface are completely covered and efficiently blocked by Cl atoms, in contrast to the highly disordered HS-AlF_3 [37].

In addition to catalytic test reactions, temperature programmed desorption (TPD) of an adsorpted base such as ammonia (NH_3-TPD) is like photoacoustic IR spectroscopy of, e.g., adsorpted pyridine (PAS/Py) also an useful tool for estimating the acid strength of solid acids. By PAS/Py discrimination between Lewis and Brønsted acidity is possible, and as shown in Fig. 2 HS-AlF_3 has almost exclusively Lewis

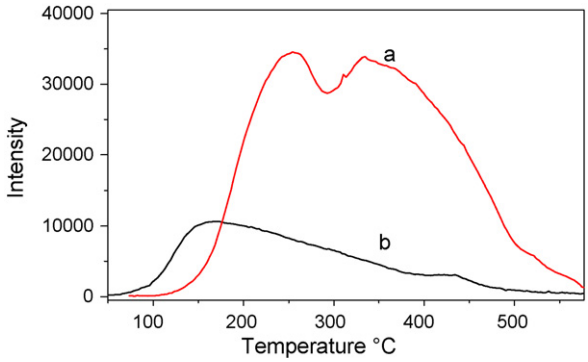

Fig. 5. NH_3-TPD of (a) HS-AlF_3 and (b) HS-AlF_3/HF (reproduced from [29] Fig. 9 by permission of Springer Publishers).

acid sites. Further on, by NH_3-TPD the strength of the acidic sites can be assessed, the more strong the sites the higher the temperature at which NH_3 will be released. The NH_3-TPD curve for HS-AlF_3 in Fig. 5 reveals expectedly a broad range of differently acidic sites, a great many of them are very strong as NH_3 becomes released up to 500 °C.

The extremely high Lewis acidity, which is obviously related to the high surface area, triggered a variety of investigation of HS-AlF_3 and also of the dry Al–F-gel. Since both are X-ray amorphous X-ray structural analyses are not possible and information had to be derived from other types of investigations, the results of which are summarised in the following.

Surface area in the range from 200 to 400 m^2/g have been found for HS-AlF_3 and up to 600 m^2/g for the dry Al–F-gel, but only HS-AlF_3 was found to be active in catalysis indicating that the extent of the surface area is not directly correlated with Lewis acidity [29]. HS-AlF_3 N_2 adsorption/desorption isotherms together with pore-size distribution are shown in Fig. 6 from which the mesoporous character can be seen.

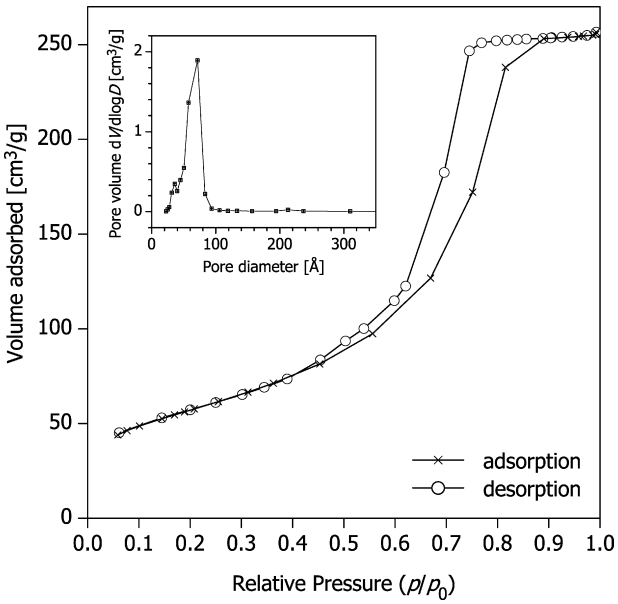

Fig. 6. N_2 adsorption/desorption isotherms and pore size distribution of HS-AlF_3 (reproduced from [21] by permission of Wiley–VCH Publishers).

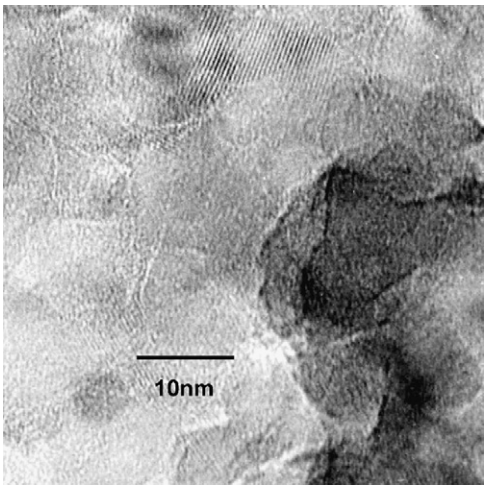

Fig. 7. TEM micrograph of HS-AlF_3 (reproduced from [21] by permission of Wiley–VCH Publishers).

HS-AlF_3 is according to TEM (Fig. 7) composed of about 10 nm sized domains, in some of which lattices planes were detected with a distance of about 3.5 Å which is typical for aluminium fluorides [21].

In its IR transmission spectrum (Fig. 8) HS-AlF_3 shows only a band at 667 cm^{-1} of the Al–F valence vibration ν_3, which is very broad as a consequence of the high degree of disorder [29].

The amorphicity and high degree of disorder of HS-AlF_3 is also obvious from its ^{27}Al-MAS-NMR spectrum (Fig. 9). It shows a single peak at −13.8 ppm, indicative for an octahedral coordination of the Al atoms, and a very broad range of sidebands from which quadrupolar coupling constant of about 1.5 MHz follows indicating a very high degree of disorder [21].

Information obtained by NMR is averaged for the bulk material but is not characteristic for the surface where the heterogeneous reactions take place. The octahedral coordination at Al found by MAS-NMR does therefore not necessarily hold for Al atoms near the surface, which instead might be under-coordinated.

Using *ab initio* computational methods the surface structures of α-AlF_3 and β-AlF_3 have been investigated [38,39]. Similar investigation of the amorphous HS-AlF_3 is not possible as it fulfils not the precondition, i.e. it does not have a regular and known bulk structure. From these investigations it follows that in α-AlF_3 all Al atoms near the surface are efficiently shielded by F atoms whereas in β-AlF_3 there are near the surface accessible five-fold coordinated, i.e. under-coordinated Al atoms, which are responsible for the known Lewis acidity of β-AlF_3. In HS-AlF_3, the ratio of surface-near Al to bulk Al is much higher than in β-AlF_3 because of the higher surface area, and there is a high degree of disorder, consequently, higher Lewis acidity has to be expected than for β-AlF_3. This is in complete agreement with the observed differences in the respective catalytic behaviour.

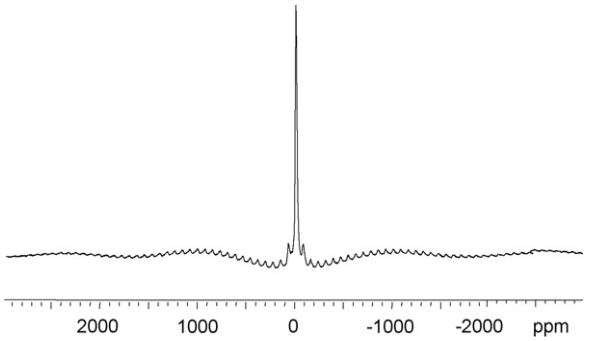

Fig. 9. ^{27}Al MAS NMR spectrum of HS-AlF_3 (reproduced from [21] by permission of Wiley–VCH Publishers).

To get information about the chemical state of Al and F in surface-near regions, HS-AlF_3 as well as the dry Al–F-gel were also characterised by XPS, which is because of the small mean free path of the photoelectrons sensitive to about 1–2 nm depth only. Of both compounds the F 1s binding energy (BE) together with the F KLL kinetic energy (KE) and the resultant modified Auger-parameter (MAP = BE + KE) are given in a Wagner plot (Fig. 10) together with the respective data of α-AlF_3 and β-AlF_3 and of aluminium hydroxyl fluoride. The Al binding energies are for HS-AlF_3 Al 2p 76.3 eV, Al 2s 121.0 eV and for dry Al–F-gel Al 2p 76.3 eV and Al 2s 121.1 eV, respectively [25].

From Fig. 10, it follows that all the investigated Al fluorides are structurally closely related as they all lie in the Wagner plot within a small corridor along the lines. Further on, a distinct

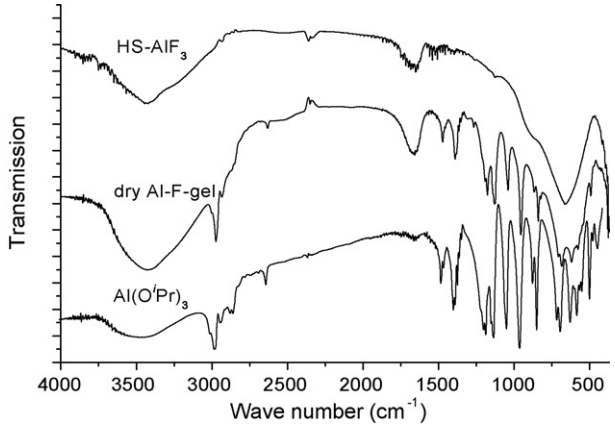

Fig. 8. IR spectra of HS-AlF_3, dry Al–F-gel and Al isopropylate (reproduced from [29] Fig. 11 by permission of Springer Publishers).

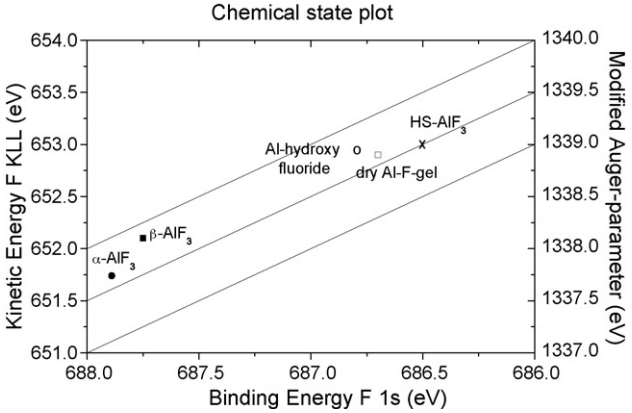

Fig. 10. Chemical state plot for F 1s orbital of aluminium fluorides (based on data taken from [25] by permission of The Royal Society of Chemistry).

shift in the binding energies can be seen with α-AlF_3 and HS-AlF_3 occupying the extreme positions as they do in their respective catalytic activity. Remarkably, the XPS data of HS-AlF_3 and its pre-form the dry Al–F-gel are rather close (fluorine) or almost identical (aluminium). This indicates that indeed the sol–gel fluorination synthesis of the dry Al–F-gel is the decisive step of HS-AlF_3 formation. The activation of the dry Al–F-gel, i.e. its conversion into HS-AlF_3, is at least in part a replacement of O^iPr ligands with F whereby most of the distortion is preserved. Although OR is replaced by the more electronegative F the electronic effect can be small assuming that not the voluminous OR but the smaller F ligand is shared between two Al centres. According to their EXAFS spectra α-AlF_3, β-AlF_3, dry Al–F-gel, dry Al–F-gel heated under inert atmosphere, and HS-AlF_3 can be divided into two groups of rather similar behaviour [40]. The first group comprises α-AlF_3, β-AlF_3 and the heated Al–F-gel with the spectra β-AlF_3 and the heated gel being very similar. In fact, β-AlF_3 is formed when dry Al–F-gel is heated over extended time under self created atmosphere. The second group comprises dry Al–F-gel and HS-AlF_3, the EXAFS spectra of which are nearly identical, which is a further evidence for their close relation. This similarity indicates that disorder pre-formed in the precursor is the reason for the high Lewis acidity of HS-AlF_3. The EXAFS spectra support the view that in going from crystalline AlF_3 over dry Al–F-gel to HS-AlF_3 there is a decrease in Al coordination number with HS-AlF_3 significantly differing from the others [40]. Indeed, five-fold coordinated Al can be stable as shown by the *ab initio* calculations for the surface of β-AlF_3 [39].

3.3.1. Catalytic properties of HS-AlF_3

The most outstanding property of HS-AlF_3 is its extremely high Lewis acidity. Due to this, it has potential as catalyst for reactions, which are known to be catalysed by strong Lewis acids. On the other hand the strongest Lewis acid centres are most likely to become blocked thereby deactivating the catalyst by reaction with, e.g., HF or H_2O, which might be formed in course of the reaction. Although the HS-AlF_3 can be easily re-activated [21] the reaction to be catalysed will not proceed. Till now, just a limited number of catalysed reactions have been investigated, a part of which have already been discussed (Eqs. (7)–(10)). In addition, isomerisation of 1-butene and of *o*-xylene have been reported [29].

HS-MgF_2: The non-aqueous sol–gel fluorination synthesis of magnesium fluoride follows basically the general route described above, however, because of much lower Lewis acidity of Mg^{2+} compared to Al^{3+} the carbon content of the dry Mg–F-gel can be that low that there is no general need for a second fluorination step [26]. Under-stoichiometric fluorination results in isolable magnesium methoxo fluorides of the type $Mg(OCH_3)_{2-x}F_x$, which are hydrolysable to the corresponding hydroxy/oxo fluorides. But complete fluorination gives also nano-structured amorphous magnesium fluoride with high surface area. After calcinations at 700 °C XRD pattern confirm the known rutil structure of MgF_2.

Magnesium fluoride prepared via sol–gel fluorination is X-ray amorphous or shows only very broad peaks in its X-ray diffraction pattern and has a very high surface area (HS-MgF_2) ranging from 150 to 350 m^2/g, in strong contrast to 0.4 m^2/g of commercial MgF_2 [26]. Fig. 11 shows BET-N_2 adsorption–desorption isotherms together with the pore size distribution of a HS-MgF_2 sample with 218 m^2/g surface area.

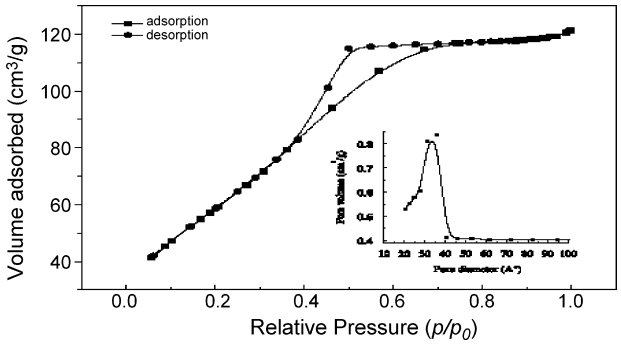

Fig. 11. HS-MgF_2 N_2 adsorption–desorption isotherms and pore size distribution (reproduced from [26] by permission of Elsevier Publishers).

XPS investigations of the almost amorphous HS-MgF_2 and of commercial crystalline MgF_2 show structural similarity of the two, however, binding energies and modified Auger parameters of the two materials are not identical. The Mg 1s binding energy of HS-MgF_2 is shifted to somewhat higher value, indicating an increased positive charge and, consequently, increased Lewis acidity at the Mg ions [26].

Although MgF_2 is known to exhibit some Lewis acidity [41] the acidity is much weaker than to expect for the Mg^{2+} ion. This is due to almost complete shielding of Mg^{2+} in the regular, crystalline MgF_2. However, similar to HS-AlF_3, in the amorphous HS-MgF_2 there will lattice distortions occur resulting in partial under-coordination of surface-near Mg^{2+}, which become this way accessible to reactants. In fact, Lewis acidity has been detected in HS-MgF_2 by NH_3-TPD. However, samples heated up to 500 °C did not show such acidity, obviously because of crystallisation, which is reported to occur at 392 °C (Fig. 12). The catalytic performance of HS-MgF_2 has been tested with the dismutation of $CHClF_2$ (Eq. (8)) because this reaction depends on Lewis acidic catalyst. The conversion observed (3% at 300 °C; 60% at 350 °C) is indicative for weak to moderate Lewis acidity [26].

The ^{19}F MAS-NMR resonance signal of HS-MgF_2 (−198.7 ppm) was found to be at almost identical position compared to that of crystalline MgF_2 (−198.5 ppm), i.e. the coordination numbers are in average identical. The broader line-width of HS-MgF_2 gives evidence for its structural distortion. Similar conclusions have been drawn from IR spectra of HS-MgF_2 (Mg–F stretch ν_1 at 450 cm^{-1}; bending δ at 260 cm^{-1}) where the broadening of the adsorption bands are likewise explained with structural disorder [26].

The first report on a thin film metal fluoride prepared via non-aqueous sol–gel fluorination was about MgF_2 [26,42]. A clear MgF_2 sol of low viscosity was prepared by the reaction of Mg methoxide in MeOH with HF/MeOH solution. This sol was successfully used for dip- as well as spin-coating of Si and SiO_2 plates. Clear transparent layers were obtained after calcinations,

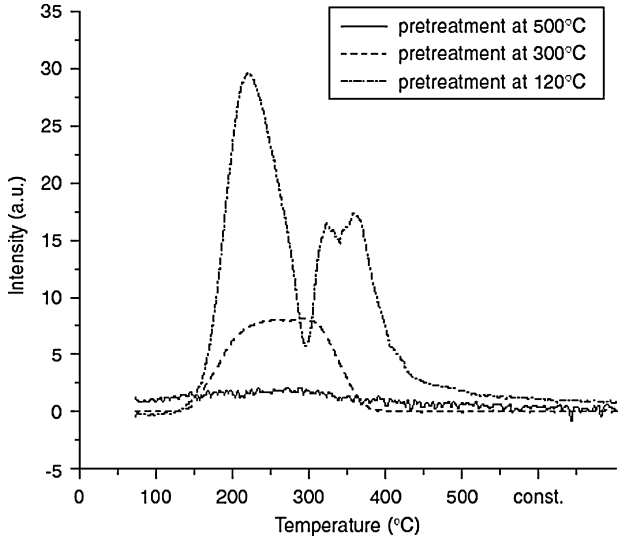

Fig. 12. NH_3-TPD of HS-MgF_2 preheated at different temperatures (reproduced from [26] by permission of Elsevier Publishers).

the thickness of which (19–222 nm) corresponded to the number of repeated coatings and concentration of the sol.

HS-CaF_2 [36]: The synthesis via non-aqueous sol–gel fluorination followed the principal route described. $Ca(OEtOMe)_2$ was reacted in MeOEtOH solution with HF/MeOEtOH yielding a sol, which became upon distilling off of some MeOEtOH a gel and eventually a white solid, dry Ca–F-gel. The dry Ca–F-gel gave in XRD very broad reflexes matching those of synthetic fluorite (PDF 4-864), and its surface area was 324 m^2/g. The material showed in contrast to HS-MgF_2 no catalytic activity for $CHClF_2$ dismutation up to 400 °C indicating absence of Lewis acid sites.

LiF, NaF, KF, and CsF: The syntheses followed the general route described starting from the respective alkali *tert*-butoxides in THF solution reacted with HF in diethylether. Only in case of LiF and NaF a gel was primarily formed while KF and CsF precipitated immediately [28]. After removing the solvent, in all cases crystalline alkali fluorides were obtained.

3.4. Examples of fluorometallates

Various fluoroaluminates of the type $MAlF_4$, M_3AlF_6 and $M_5Al_3F_{14}$ have been formed by sol–gel reaction from their metal alkoxides [28].

Synthesis of the complex metal fluoroaluminates was carried out according to the following equation:

$$\begin{aligned} &mM^{I}O^{t}Bu + nAl(O^{t}Bu)_3 \\ &\quad + (m+3n)HF(Et_2O) \rightarrow M^{I}_{m}Al_nF_{(m+3n)} \\ &\quad + (m+3n)^{t}BuOH \\ &(m=n=1; M^{I}=K, Cs; \quad m=3, n=1; M^{I}=Li, Na, K) \end{aligned} \tag{11}$$

Different molar compositions of M^I:Al and varying cations resulted in compounds of the elpasolite type, which are studied by temperature programmed XRD, solid state ^{19}F and ^{27}Al NMR and thermal analysis. Thin films from the sol state of cryolites were obtained by dip-coating. SEM images show high homogeneity of particles, AFM measurements allowed the estimation of size in the range of 300–500 nm (Fig. 13).

Complex fluoroaluminates as cryolite and chiolite exhibit excellent optical properties: refractive index at 1.33, light transmission occurs in a wide range of 150–14,000 nm. Cold pressing of this material at 10 t/cm^2 gave transparent plates.

Complex fluorides of the earth metals as $KMgF_3$, K_2MgF_4 and $BaMgF_4$ are obtained as powder or thin film coatings at room temperature by sol–gel fluorination, while the conventional method of high temperature melting of fluorides affords 600–800 °C over longer time in inert atmosphere of closed platinum tube [43]. $BaMgF_4$ is of special importance because of its ferroelectric properties. Simply, barium- and magnesium methoxides are mixed in 1:1 molar ratio in methanol and are then reacted with four equivalents of HF/CH_3OH. Evaporation of the solvent results in an X-ray amorphous solid, which upon calcination at 600 °C shows the XRD pattern of the crystalline complex fluoride.

This synthesis method holds also for $CaAlF_5$ and $BaAlF_5$ [44].

3.5. Examples of doped metal fluorides

Cationic doping: It is known that partial substitution of the metal cations (“doping”) alters the catalytic properties of a solid metal compound. For metal oxides this has been explained by Tanabe’s model [45], which has been extended to metal fluorides [46]. According to the model partial substitution of M^{n+} by

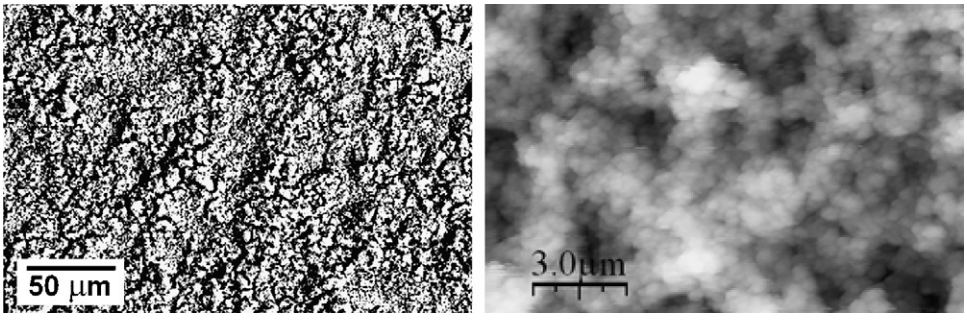

Fig. 13. Films of Na_3AlF_6–sols. Left, SEM of glass coating; right, AFM of coating on Si (reproduced from [28] by permission of Elsevier Publishers).

$M^{(n+1)+}$ cations creates at the $M^{(n+1)+}$ site an excess charge of +1 (which is balanced within the solid) and, consequently, Lewis acidity. Necessary preconditions are comparable size of the cations and appropriate concentrations, as only up to a maximum of 30 mol% of the dopant can become incorporated into the host maintaining the lattice of the latter [22].

The non-aqueous sol–gel fluorination synthesis provides convenient access to mixed metal fluorides by simply starting from admixtures of alkoxide or other appropriate metal compound solutions, which are fluorinated as described above. This way the dopant metal fluoride becomes finely distributed in the matrix of the host metal fluoride having a high surface area.

Magnesium fluoride has been extensively used as host for MF_3/MF_2 doping systems. The dopant metal compound can be an alkoxide, however, other compounds can also be used as shown below, broadening the scope of the method in case the respective alkoxides are not or not easily available. HS-MgF_2 can be easily prepared, has negligible Lewis acidity, and the size of the Mg^{2+} ion (0.72 Å) is appropriate for several M^{3+} ions. Thus with M^{3+} = Ga, In, Fe, and V syntheses of MF_3/MgF_2 doped systems have been carried out based on the non-aqueous sol–gel fluorination [22]. The syntheses started from $Mg(OMe)_2$ and MCl_3 or $In(O^iPr)_3$, respectively, with 15 mol% of the M^{3+}, as this concentration had proved to result in maximum effect [47]. The surface areas of the doped systems varied from 100 to 155 m^2/g, i.e. up to three times that of conventionally prepared materials. In X-ray diffraction patterns showed rather broad peaks of MgF_2 only. In accordance with the theoretical model [46] the photoacoustic FT-IR spectra of adsorbed pyridine gave evidence for Lewis acidity (band at 1451 cm^{-1}) of the doped systems but not of MgF_2. More detailed investigations of the Ga doped materials by X-ray photoelectron spectroscopy (XPS/XAES) revealed close structural uniformity of HS-MgF_2, MgF_2, sol–gel prepared Ga^{3+} doped HS-MgF_2 and conventionally via aqueous route prepared Ga^{3+} doped MgF_2. Obviously, the Ga^{3+} ions became incorporated in the MgF_2 lattice without causing substantial changes. The doped M^{3+}/MgF_2 systems were tested in standard reactions for their performance as catalysts. In CCl_2F_2 dismutation (Eq. (7)) the vanadium doped catalyst was rather active, whereas the other catalysts were active in benzoylation of anisole (Eq. (12)) (100% conversion, in contrast to zero conversion with, e.g., pure $GaCl_3$). The Fe doped catalyst was also highly active in alkylation of benzene (Eq. (13)) (100% conversion) and in hydrofluorination of tetrachloroethylene (Eq. (14)) [22]:

$$CH_3OC_6H_5 + C_6H_5C(O)Cl \rightarrow CH_3OC_6H_4{-}C(O)C_6H_5 + HCl \quad (12)$$

$$C_6H_6 + C_3H_7Cl \rightarrow C_6H_5{-}C_3H_7 + HCl \quad (13)$$

$$nCCl_2CCl_2 + mHF \rightarrow CF_3CHCl_2 + CF_3CHClF + CF_3CHF_2 + \text{others} \quad (14)$$

The Fe^{3+} doped MgF_2 system was investigated in more detail [23]. Samples of 15 mol% Fe^{3+} in MgF_2 prepared from different sources of Fe^{3+} ($FeCl_3$, $Fe_2(SO_4)_3$, $Fe(OMe)_3$) were post-fluorinated with CCl_2F_2 as well as with HF and the resulting catalysts compared with each other. All catalysts had high surface areas, the HF post-fluorinated were superior in this respect, most likely due to the lower fluorination temperature needed (120 °C versus 350 °C). On the other hand PAS of adsorbed pyridine showed for HF post-fluorinated material a somewhat lower Lewis acidity compared to respective material which was CCl_2F_2 post-fluorinated, corresponding to what was reported for HS-AlF_3 (see above).

From CCl_2F_2 dismutation and NH_3-TPD it follows that the $Fe(OMe)_3$ based and CCl_2F_2 post-fluorinated catalyst was the most Lewis acidic one, which, however, was not at all active in hydrofluorination of C_2Cl_4, and also not in isomerisation of CHF_2CHF_2 to CF_3CH_2F, since the latter proceeds via HF splitting off followed by anti-Markownikov addition of HF to the intermediate [23]. This is explained by the fact that the strongest Lewis acid sites are the ones which are most efficiently blocked by HF. Catalysts of lower performance in NH_3-TPD were, however, quite active for the hydrofluorination reaction.

From the reported results with the Fe^{3+} doped MgF_2 catalysts it was concluded that sol–gel synthesis of doped systems opens possibilities for obtaining ‘‘tailored’’ catalysts.

Chromium(III) doped magnesium fluoride catalysts have also been prepared and thoroughly investigated [24]. The syntheses followed the general route starting from $Mg(OMe)_2$ in MeOH and $CrCl_3$, $Cr_3(CH_3COO)_7(OH)_2$, or CrO_3 as Cr^{3+} precursors, whereby CrO_3 was prior reduced and dissolved by reacting with methanol. The post-fluorination/activation was done with CCl_2F_2 up to 350 °C. X-ray diffraction patterns of all preparations showed only very broad reflexes attributable to MgF_2, that gives evidence for Cr^{3+} being incorporated into the MgF_2 lattice rather than forming separate phases. Consequently, the expected Lewis acidity has also experimentally been confirmed with PAS of chemisorbed pyridine. ESCA surface analysis of a number of Cr^{3+} doped catalysts monitoring binding energies of core levels and kinetic energies of Auger electrons evidenced structural similarity of all catalysts and of MgF_2.

The Mg 1s and F 1s binding energies of the catalysts (see Fig. 14) were rather close together but shifted to lower binding energy compared to the respective values of MgF_2 suggesting that the chemical surroundings of Mg and F in the Cr^{3+} doped catalysts differ from those in MgF_2. A lower binding energy of an atom indicates increased electron density at this atom, i.e. increased Lewis basicity. For the Cr atoms in the catalysts Cr 2p binding energies around 578.5–579.7 eV were found, correlating well with the 579.7 eV measured with α-CrF_3 but substantially higher than for CrO_3 (576.2 eV) [24]. Corresponding to the gain in electron density at Mg and F there is obviously a loss in electron density at Cr, i.e. an increase of Lewis acidity. Another conclusion drawn is that there is no chromia phase but Cr^{3+} is occupying Mg^{2+} lattice places with F atoms next to it.

Selected Cr^{3+}/MgF_2 catalysts were tested with two reactions, i.e. dismutation of CCl_2F_2 (Eq. (7)) and dismutation of

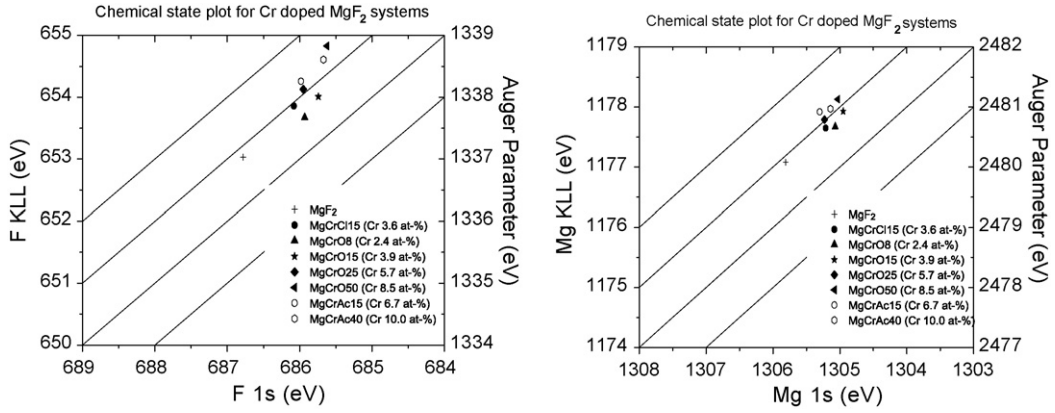

Fig. 14. Chemical state plots for F 1s and Mg 1s orbitals of chromium(III)-doped MgF_2 (reproduced from [24] by permission of Elsevier Publishers).

CF_3CHClF (Eq. (15)). The results are given in Figs. 15 and 16:

$$2CF_3CHClF \rightarrow CF_3CHCl_2 + CF_3CHF_2 \quad (15)$$

It can be seen from Figs. 15 and 16 that the catalyst denominated CrOMg15 (i.e. from CrO_3 precursor with 15 mol% Cr^{3+}) had in both reaction the highest performance, indicating once more that 15% doping is optimum.

Anion doping: Adopting the Tanabe model analogously for anion doping, the substitution of a monovalent fluoride anion by a di- or higher valent anion should result in Lewis basicity. That principle was exemplarily tested for magnesium fluoride [32,27]. The sol–gel fluorination route can be conveniently used to modify the anionic composition of metal fluorides. If the metal alkoxide is reacted with smaller amounts of anhydrous HF solution than needed by stoichiometry, unreacted alkoxide groups will remain. The latter can be used to modify the material. Basically, the syntheses described in [27] followed the general scheme. Magnesium methoxide, freshly prepared from Mg and MeOH, in MeOH was reacted with defined under-stoichiometric amounts of HF/Et_2O, the gel was dried and finally calcined at 350 °C for 3 h to convert the residual methoxide groups into oxidic ones. In another procedure used, wet Mg–F-gel prepared with stoichiometric amounts of HF was subsequently partially hydrolysed by adding measured amounts of water. Again, the dry gel was calcined. This way materials with analytical F:Mg ratios equal to 0.3, 0.5, 0.8, and 0.9 and surface areas from 278 to 387 m^2/g were prepared. In XRD these magnesium oxide fluorides showed very weak and broad reflexes of MgO and/or MgF_2, whereas analogously calcined HS-MgF_2 gave more distinct MgF_2 reflexes. From ^{19}F MAS NMR investigations it could be concluded that three-fold coordinated F atoms as they are in crystalline MgF_2 are also prevailing in sol–gel prepared calcined MgF_2, but became less dominant with decreasing F content of the materials. There is a shift to higher ppm values, which is explained as resulting from Mg–F bond lengths becoming longer. XPS surface analysis gave evidence for Mg 1s binding energy shifted to lower values with decreased F content, i.e. the Lewis acidity decreases with decreased F content as expected. The catalytic activity of these materials was tested with Michael addition reactions, which are known to need basic catalysis. Heterogeneously catalysed additions of

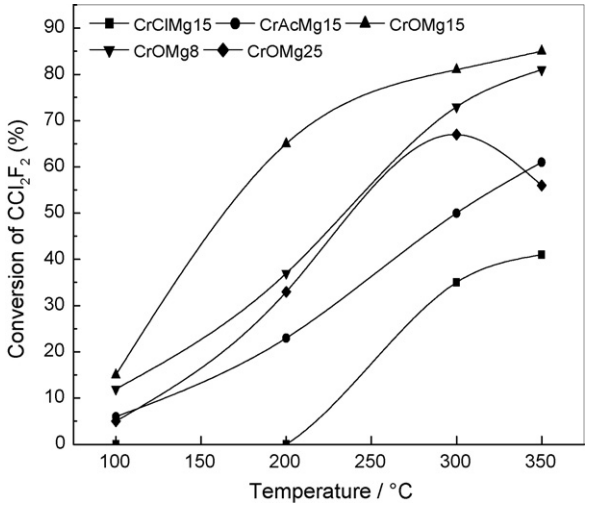

Fig. 15. Dismutation of CCl_2F_2 over Cr^{3+}/MgF_2 catalysts (reproduced from [24] by permission of Elsevier Publishers). CrClMg15: 15 mol% Cr, $CrCl_3$ precursor, S_{BET} 106 m^2/g; CrAcMg15: 15 mol% Cr, $Cr_3Ac_7(OH)_2$ precursor, S_{BET} 65 m^2/g; CrOMg15, CrOMg8, CrOMg25: 15, 5, or 25 mol% Cr, CrO_3 precursor, S_{BET} 175, or 167, or 99 m^2/g.

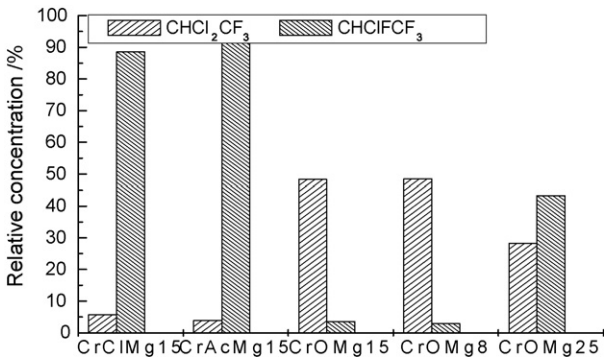

Fig. 16. Dismutation of $CHClFCF_3$ over Cr^{3+}/MgF_2 catalysts (reproduced from [24] by permission of Elsevier Publishers). Catalysts same as in Fig. 15. (The reaction was followed by ^{19}F NMR of products solution in $CDCl_3$. Due to its high vapour pressure CF_3CHF_2 was not completely recovered, hence it was omitted in the figure)

methyl vinyl ketone to 2-methylcyclohexane-1,3-dione (Eq. (16)), to 2-acetylcyclopentanone and 2-acetylcyclohexanone (Eq. (17)), and to 2-methoxycarbonylpentanone (Eq. (18)) were studied:

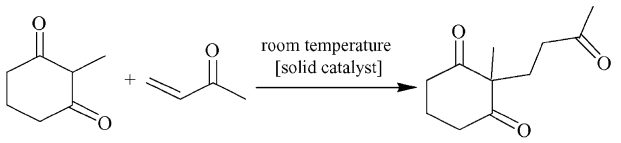

(16)

2-(3-oxobutyl)-
2-methylcyclohexane-1,3-dione

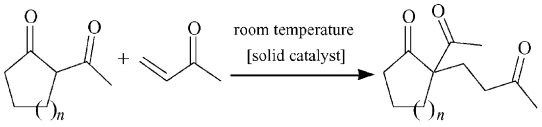

(17)

$n = 1$: 2-acetyl-2-(3-oxobutyl)-cyclopentanone
$n = 2$: 2-acetyl-2-(3-oxobutyl)-cyclohexanone

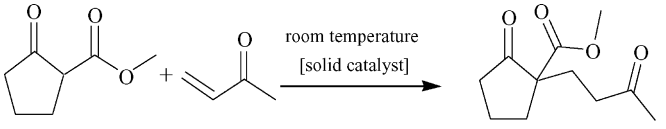

(18)

2-oxo-1-(3-oxo-butyl)-
cyclopentanecarboxylic acid methyl ester

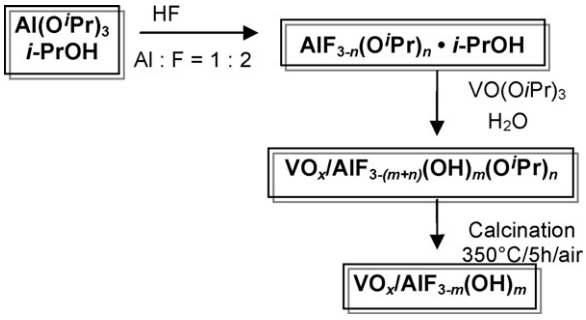

Scheme 5. Preparation of AlF_3-supported VO_x oxidation catalyst.

Pure crystalline MgF_2 was catalytically not active, whereas MgO was very active but gave low yields because of extensive consecutive reactions. Superior results are reported for a magnesium oxide fluoride with an F:Mg ratio of 0.9, which gave best yields because of high selectivity and no consecutive reactions [27]. Obviously, by anion doping a bifunctional solid catalyst with both Brønsted base and Lewis acid sites had been created, giving optimum preconditions for both activity and selectivity for Michael additions [27].

3.6. Metal fluorides as support or dispersion medium for catalytically active materials

The use of metal fluorides as supports for active species in catalysis describes a principle where the gel state of metal fluoride preparation is advantageously employed to anchor such groups or dispersing them in a matrix. Additionally, a Lewis acidic support may gradually improve the performance of the active principle, as also high surface area and the homogeneity of dispersion do [48].

As a new approach to supported catalysts, the fluorination of Al alkoxide is carried out with two equivalents of HF only, while the remaining Al-OR anchor group is used for functionalization by vanadyl alkoxide according to Scheme 5. This way, the VO_x-species are homogeneously dispersed in the AlF_3 matrix, which has exclusively Lewis acidic sites without any Brønsted acidity. The obtained catalyst is mesoporous with surface areas in the range of 140–165 m^2/g. From MAS NMR, FT-IR and Raman data was a structure proposed [48], which is shown as part of Scheme 6.

The structure model describes the intermediate complex from which propene and water as products are formed. The highest yield of propene is achieved with a vanadium content of 9.5 mol% [48]. Remarkably, the selectivity of the product is higher than that of the by-products CO and CO_2, which has never been achieved with metal oxide based catalysts (see Fig. 17).

Further applications using MgF_2 and AlF_3 as supports consist in the dispersion of noble metals as platinum and palladium for dehydration reactions. One successful example is the C–C– bond formation by Suzuki coupling [49].

4. General applications

For several applications metal fluorides are superior to metal oxides. However, chemical and especial technological reasons,

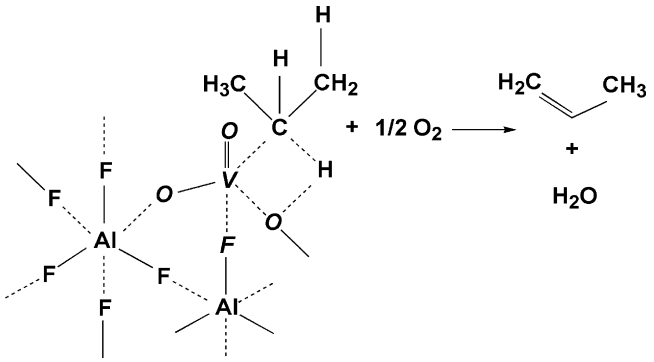

Scheme 6. Structure model of oxidative dehydrogenation of propane (reproduced from [48] by permission of The Royal Society of Chemistry).

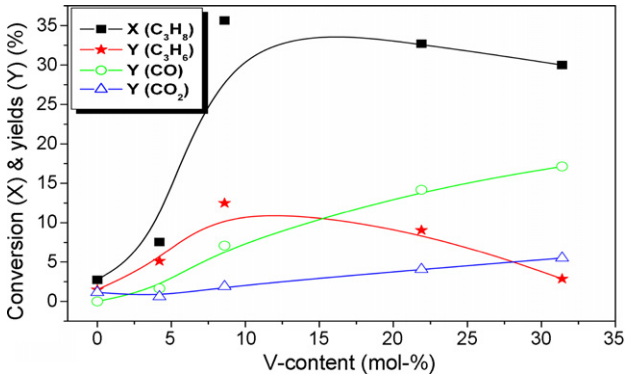

Fig. 17. Conversion of propane to propene and products of total oxidation CO and CO_2 (reproduced from [48] by permission of The Royal Society of Chemistry).

due to problems in processing, limit their use. The non-aqueous sol–gel fluorination synthesis described here overcomes technologic borders regarding processing and, hence, opens several new fields of applications for metal fluorides.

Selected are those applications, which are described in literature for conventional fluorides, and those of own experience and experimental research.

The versatile applications of metal fluorides are traced back to their individual properties, which strongly differ whether they are of conventionally crystalline origin or if resulting from the sol–gel-fluorination process recently established [21,30]. A priori, the latter is superior due to properties inherent of nano-structured materials as already discussed.

Thus, the surface effect and size quantization are fundamental in this respect.

Because of their morphological characteristics of nanosized and mesoporous structures the metal fluorides of the sol–gel process provide extraordinary high surface areas up to 500 m^2/g with pores in the diameter range of 10–40 Å. In case of strong Lewis acidic metal fluorides they can be advantageously used as acid catalysts.

4.1. Catalysis and acidity

Principally, metals with available LUMO orbitals and accessible metal sites show Lewis acidity. HS-AlF_3 as a distorted aluminium fluoride with under-coordination in the surface exhibit Al sites of very strong acidity, comparable with that of the strongest Lewis acids known. Therefore, it has high catalytic activity in isomerisation and dismutation reactions of halocarbon compounds as had been shown [21,30]. In many practical cases the extraordinary strong sites of "high surface AlF_3" need to be adjusted in reactivity to fit to the specific reactant molecule.

To adjust reactivity, fine-tuning of a catalyst system is achieved by doping according to the modified Tanabe model as with the three-valent metals Fe^{III}, Cr^{III}, Ga^{III} in a metal fluoride matrix [22–24]. High conversion was found for HF hydro-fluorination of C_2Cl_4 with $Fe^{III}F_3$ doped MgF_2 [23]. In contrast to the mentioned cation doping, also anion doping with oxygen for fluorine was realised to get basic catalysts of the type $Mg(O, F)_2$ from intermediate $Mg(CH_3O, F)_2$ species. The catalyst was adjusted concerning the catalytic properties and tested with good results in Michael addition reactions [27].

Another route of tuning the activity of catalysts consist in application of metal fluorides as supports, e.g., for VO_x-species by reactive anchoring. The catalyst with 9.5 mol% VO_x was successfully tested in oxidative dehydrogenation of propane [48].

4.2. Optical properties

Highest electronegativity of fluorine makes the dense electron shell of fluoride ion less polarizable as compared with, e.g., oxygen of the till now mostly applied metal oxides. Hence, metal fluorides exhibit optical properties as very low refractive indices of 1.33–1.60 and IR/UV light transmission ranges from 100 to 15,000 nm, combined with ultra low energy loss in fluoride glass material. Besides wide optical windows, selected UV/VIS absorption of metal oxy fluorides as $TiOF_2$ prevents organic material and plastics for ageing decomposition.

Optical coating achieved by thin layer films from a chemically based sol, e.g., of an MgF_2 sol [26,31], can be used in antireflective coating as well as the complex fluoroaluminates cryolite and chiolite [28].

Metal fluoride coating from diluted sol solutions of known concentrations gives reproducible MgF_2 films of 15–50 nm thickness by operating with a commercial spin coater. By manifold repetition of coating overall film thickness up to 400 nm is reached. Roughness of 4–15 nm is measured by AFM including nanoparticle diameter from 10 to 40 nm. Optical properties are measured by spectroscopic ellipsometry [42].

This opens a perspective of fluoride coating at moderate temperatures and low stress, avoiding the drawbacks of the PVD state of the art processes as plasma processing, sputtering, etc.

4.3. Coating

Metal fluoride thin film coating may serve as protective coating of sensitive metal surfaces. Improvement of surface properties of electronic parts and of tools as roughness, hydrophobicity, repellence and medical sterility is the goal of such treatments. Reactive coatings with fluorides having Lewis acidic properties as, e.g., AlF_3 are appropriate on metal surfaces of micro-reactors to initiate surface catalytic reactions. Also, inert carriers as alumina are coated with an AlF_3 sol to give an active shell type catalyst. Besides catalytic applications the high surface area in combination with active sites gives preference for use as adsorptive material.

4.4. Ceramics

At 8–10 kbar cold pressed nano-structured metal fluorides as, e.g., MgF_2, AlF_3, Na_3AlF_6 and others, give transparent ceramic plates, which may open an alternative route to transparent glassy metal fluorides. Metal fluoride coating of oxide ceramics can reduce the sintering temperature and grain boundaries of pressed powders [50].

Besides binary fluorides, complex fluorometallates of the general metal cation compositions M^I/Me^{III} (Na_3AlF_6), M^I/M^{II} ($KMgF_3$, K_2MgF_4), M^{II}/M^{II} ($BaMgF_4$), M^{II}/M^{III} ($BaAlF_5$) are accessible by the sol–gel fluorination route at room temperature. Their known optical, magnetic and ferroelectric properties are of great interest as well as their ability to host 3d transition metal- and rare-earth metal ions for luminescence.

5. Conclusion

Reflecting the scientific literature, an explosive growth of research activities on nano-sized metal fluorides has started over the past 5 years. This is mainly caused (i) by technological demands because metal fluorides are for several applications as, e.g., for optics, surface coating, and catalysis, respectively, excellent alternative materials as compared to their oxidic counterparts. The activities are further promoted by the fact (ii) that recently several new synthesis routes toward nano-sized metal fluorides have been developed giving access to these materials. Sol–gel syntheses and especially the non-aqueous sol–gel strategy as described in this article offer a wide access to different types of metal fluorides with reasonable efforts. However, this synthesis strategy is a very new one and needs further development and exploration in order to access full potential for possible technological applications. Hence, it is a challenging task to investigate in detail the synthesis mechanism, and this way, to apply this strategy even on transition metal fluorides and complex fluorometallates, which are of high interest for Laser and luminescence applications. Moreover, it is still a somehow open point what impact the drastic decrease of the particle size down to the low nanometer scale, and combined with this the drastic increase of surface area, on the surface properties of the nano-structured metal fluorides have, e.g., in case of HS-AlF_3 it has been undoubtedly proven that the Lewis acidity has drastically increased with surface area, being comparable with that of SbF_5, the strongest Lewis acid known so far. As a result, any electron donor molecule will be more or less tightly bind (adsorbed) on the strongly Lewis acidic surface sites. No wonder, that HS-AlF_3 binds water molecules very tightly, and it is still not understood, which consequences it might have on surface properties. In case of Lewis acidity, it evidently has a negative impact. As a consequence of this, non-hygroscopic, that is non-Lewis-acidic, metal fluorides have to be found and synthesized this way which might be used for applications beyond catalysis. There are several metal fluorides responding to this demand, especially complex metal fluorides are known to be neutral because of the close packing of F-ions and strong octahedral coordination of all the metals involved in the structure building. Fortunately, our first investigations evidently prove that complex metal fluorides are accessible via the non-aqueous synthesis route already at room temperature whereas in the classical synthesis route these materials can be prepared just by high temperature reaction of the respective binary metal fluorides. Hence, it is obvious that synthesis strategies based on aqueous syntheses are not suitable for such applications.

A further impact coming from this new non-aqueous sol–gel-synthesis is the fact that most of the metal fluorides can be obtained not only in the nano-dimension but they are almost X-ray amorphous. Hence, this opens a wide field for the use of these X-ray amorphous fluoride powders for the synthesis of various fluoride glasses. Even the production of transparent metal fluoride ceramics using nano-sized metal fluoride powders as an interesting alternative to the respective metal fluoride single crystals should be possible.

As was successfully shown for the Mg–F–O system the OR against F-exchange can be stopped at any intermediate stoichiometric ratio thus resulting in highly amorphous oxide fluorides, which are not at all available via any other synthesis route so far. Such compounds may be of interest for both, catalysis as well as optics.

An almost unexplored field is the functionalization of nano-fluorides by leaving a defined number of OR-groups unconverted to use them as chemical anchors to bind any other compounds on it. This gives access to metal fluoride-inorganic as well as metal fluoride-organic hybrid systems as it has been developed for many metal oxides. Hence, achievements in the nano metal oxide systems should be principally applied to metal fluorides giving access to materials and application, which, at this time, cannot be foreseen.

Besides searching for new applications of nano metal fluorides accessible via this new non-aqueous sol–gel synthesis, there is still a lot of fundamental research to do aiming at understanding the chemistry, which is going on in detail. Since most of these materials are X-ray amorphous it is also a challenging task to explore and to apply powerful diagnostic techniques like solid state MAS-NMR, EXAFS, XANES, etc. to understand the mechanism of the reactions involved.

Based on this synthesis strategy and new applications resulting from it metal fluorides will very probably experience a renaissance in sciences and technology in the next future.

Note added in proof

While the manuscript was already finished, a paper appeared in Phys. Chem. Chem. Phys. 8 (2006), 5045 by S. Chaudhuri, P. Chupas, B.J. Morgan, P.A. Madden and C.P. Grey, describing by molecular dynamics calculation the drastic changes of properties in going from bulk AlF_3 to nano-sized AlF_3.

Acknowledgements

This work was supported by the EU 6th Framework Program (FUNFLUOS, Contract no. NMP3-CT-2004-5005575) and, partly by the Deutsche Forschungsgemeinschaft (DFG), project Ke 489/22.

References

[1] P. Yang (Hrsg.), The Chemistry of Nanostructured Materials, World Scientific Publ., Singapore, 2003.
[2] P. Thangadurai, S. Ramasamy, R. Kesavamoorthy, J. Phys.: Condens. Mater. 17 (2005) 863–874.

[3] H. Guérault, J.M. Greneche, J. Phys.: Condens. Mater. 12 (2000) 311–322.
[4] T.S. Korolyova, M.M. Kidibaev, B.K. Dzholdoshov, J. Phys. Stat. Sol. 47 (2005) 1417–1419.
[5] L.J. Ling, A.D. Berry, A.P. Purday, Thin Solid Films 209 (1992) 9–16.
[6] G.G. Condorelli, S. Gennaro, I.L. Fragata, Chem. Vapour Depos. 7 (2001) 151–156.
[7] S.V. Kuznezov, V.V. Osiko, E.A. Tkatchenko, P.P. Fedorov, Russ. Chem. Rev., in press.
[8] S. Sakka (Hrsg), Handbook of Sol–Gel Science and Technology, Kluwer, Boston, 2005.
[9] A.M. Mailhot, A. Elyamani, R.E. Riman, J. Mater. Res. 7 (1992) 1534–1540.
[10] M. Saad, M. Poulin, J. Non-Cryst. Solids 184 (1995) 352–355.
[11] M. Dejneka, E. Snitzer, R.E. Riman, J. Non-Cryst. Solids 202 (1996) 23–34.
[12] J. Ballato, M. Dejneka, R.E. Riman, E. Snitzer, W. Zhou, J. Mater. Res. 11 (1996) 841–849.
[13] R.E. Riman, in: L.C. Klein (Ed.), Sol–Gel Optics: Processing and Applications, Kluwer, Norwell, 1994, p. 197.
[14] H.-X. Mai, Y.-W. Zhang, R. Si, Z.-G. Yan, L. Sun, L.P. You, C.-H. Yan, J. Am. Chem. Soc. 128 (2006) 6426–6436.
[15] J. Labeguerie, P. Gredin, J. Marot, A. De Kozak, J. Solid State Chem. 178 (2005) 3197–3205.
[16] S. Fujihara, Y. Kadota, T. Kimura, J. Sol-Gel Sci. Technol. 24 (2002) 147–154.
[17] H. Naito, S. Fujihara, T. Kimura, J. Sol-Gel Sci. Technol. 26 (2003) 997–1000.
[18] S. Fujihara, T. Kato, T. Kimura, J. Sol-Gel Sci. Technol. 26 (2003) 953–956.
[19] T. Skapin, E. Kemnitz, J. Non-Cryst. Solids 225 (1998) 163–167.
[20] S. Fujihara, Recent Res. Dev. Mater. Sci. 3 (2002) 619–631.
[21] E. Kemnitz, U. Groß, St. Rüdiger, S.C. Shekar, Angew. Chem. Int. Ed. 42 (2003) 4251–4254.
[22] J.K. Murthy, U. Groß, St. Rüdiger, E. Ünveren, E. Kemnitz, J. Fluorine Chem. 125 (2004) 937–949.
[23] J.K. Murthy, U. Groß, St. Rüdiger, E. Kemnitz, Appl. Catal. A 278 (2004) 133–138.
[24] J.K. Murthy, U. Groß, St. Rüdiger, E. Ünveren, W. Unger, E. Kemnitz, Appl. Catal. A 282 (2005) 85–91.
[25] St. Rüdiger, U. Groß, M. Feist, H.A. Prescott, S.C. Shekar, S.I. Troyanov, E. Kemnitz, J. Mater. Chem. 15 (2005) 588–597.
[26] J.K. Murthy, U. Groß, St. Rüdiger, E. Kemnitz, J.M. Winfield, J. Solid State Chem. 179 (2006) 739–746.
[27] H.A. Prescott, Z.-J. Li, E. Kemnitz, J. Deutsch, H. Lieske, J. Mater. Chem. 15 (2005) 4616–4628.
[28] M. Ahrens, G. Scholz, M. Feist, E. Kemnitz, Solid State Sci. 8 (2006) 798–806.
[29] St. Rüdiger, G. Eltanany, U. Groß, E. Kemnitz, J. Sol-Gel Sci. Technol. 41 (2007) 299–311.
[30] E. Kemnitz, U. Groß, St. Rüdiger, WO-Pat 2004060806, Method for the preparation of high surface area metal fluorides
[31] E. Kemnitz, U. Groß, St. Rüdiger, WO-Pat 2005097695, Method for the preparation of fluoride glass gel and use thereof.
[32] E. Kemnitz, U. Groß, St. Rüdiger, WO-Pat 2006058794, Method for the preparation of X-ray amorphous or weakly crystalline metal oxide fluorides.
[33] E. Kemnitz, St. Rüdiger, U. Groß, in: Proceedings of the 2nd International Siberian Workshop on Advanced Inorganic Fluorides, Tomsk, Russia, June 11–16, (2006), pp. 100–102.
[34] I. Bucsi, B. Török, A.I. Marco, G. Rasul, G.K.S. Prakash, G.A. Olah, J. Am. Chem. Soc. 124 (2002) 7728–7736.
[35] H. Thoms, M. Epple, H. Viebrock, A. Reller, J. Mater. Chem. 5 (1995) 589–594.
[36] St. Rüdiger, U. Groß, E. Kemnitz, unpublished results.
[37] J.K. Murthy, U. Groß, St. Rüdiger, V.V. Rao, V.V. Kumar, A. Wander, C.L. Bailey, N.M. Harrison, E. Kemnitz, J. Phys. Chem. B 110 (2006) 8314–8319.
[38] A. Wander, B.G. Searle, C.L. Bailey, N.M. Harrison, J. Phys. Chem. B 109 (2005) 22935–22938.
[39] A. Wander, C.L. Bailey, B.G. Searle, S. Mukhopadhyay, N.M. Harrison, Phys. Chem. Chem. Phys. 7 (2005) 3989–3993;
See also: A. Wander, C.L. Bailey, S. Mukhopadhyay, B.G. Searle, N.M. Harrison, J. Mater. Chem. 16 (2006) 1906–1910.
[40] S.L.M. Schroeder, N. Weiher, Phys. Chem. Chem. Phys. 8 (2006) 1807–1811.
[41] M. Wojciechowska, M. Zielinsky, M. Piotrowski, J. Fluorine Chem. 120 (2003) 1–11.
[42] H. Krüger, E. Kemnitz, E. Hertwig, U. Beck, Paper Presented at 18th International Symposium on Fluorine Chemistry, Bremen, Germany, 2006.
[43] M. Cao, Y. Wang, Y. Qi, C. Guo, C. Hu, J. Solid State Chem. 177 (2004) 2205–2209.
[44] U. Groß, St. Rüdiger, E. Kemnitz, unpublished results.
[45] K. Tanabe, T. Sumiyoshi, K. Shibata, T. Kiyoura, J. Kitagawa, Bull. Chem. Soc. Jpn. 47 (1974) 1064–1066.
[46] E. Kemnitz, Y. Zhu, B. Adamczyk, J. Fluorine Chem. 114 (2002) 163–170.
[47] Y. Zhu, K. Fiedler, St. Rüdiger, E. Kemnitz, J. Catal. 219 (2003) 8–16.
[48] K. Scheurell, E. Kemnitz, J. Mater. Chem. 15 (2005) 4845–4853.
[49] P.T. Patil, U. Groß, St. Rüdiger, E. Kemnitz, Paper Presented at 1st International IUPAC Conference on Green-Sustainable Chemistry, Dresden, Germany, 2006.
[50] Y. Wu, Y. Zhang, G. Pezzotti, J. Guo, Mater. Lett. 52 (2002) 366–369.